


Network pharmacology analysis of *Plumbago zeylanica* to identify the therapeutic targets and molecular mechanisms involved in ameliorating hemorrhoids

Arijit Nandi, Tanzeem Nigar, Anwesha Das & Yadu Nandan Dey


To cite this article: Arijit Nandi, Tanzeem Nigar, Anwesha Das & Yadu Nandan Dey (10 Nov 2023): Network pharmacology analysis of *Plumbago zeylanica* to identify the therapeutic targets and molecular mechanisms involved in ameliorating hemorrhoids, Journal of Biomolecular Structure and Dynamics, DOI: [10.1080/07391102.2023.2280681](https://doi.org/10.1080/07391102.2023.2280681)



To link to this article: <https://doi.org/10.1080/07391102.2023.2280681>

 View supplementary material 

 Published online: 10 Nov 2023.

 Submit your article to this journal 

 Article views: 151

 View related articles 

 View Crossmark data 

 Citing articles: 1 View citing articles 

Network pharmacology analysis of *Plumbago zeylanica* to identify the therapeutic targets and molecular mechanisms involved in ameliorating hemorrhoids

Arijit Nandi^a, Tanzeem Nigar^a, Anwesha Das^b and Yadu Nandan Dey^a

^aDepartment of Pharmacology, Dr. B.C. Roy College of Pharmacy and Allied Health Sciences, West Bengal, India; ^bDepartment of Medicinal Chemistry, National Institute of Pharmaceutical Education and Research, Ahmedabad, Palaj, Gandhinagar, Gujarat, India

Communicated by Ramaswamy H. Sarma

ABSTRACT

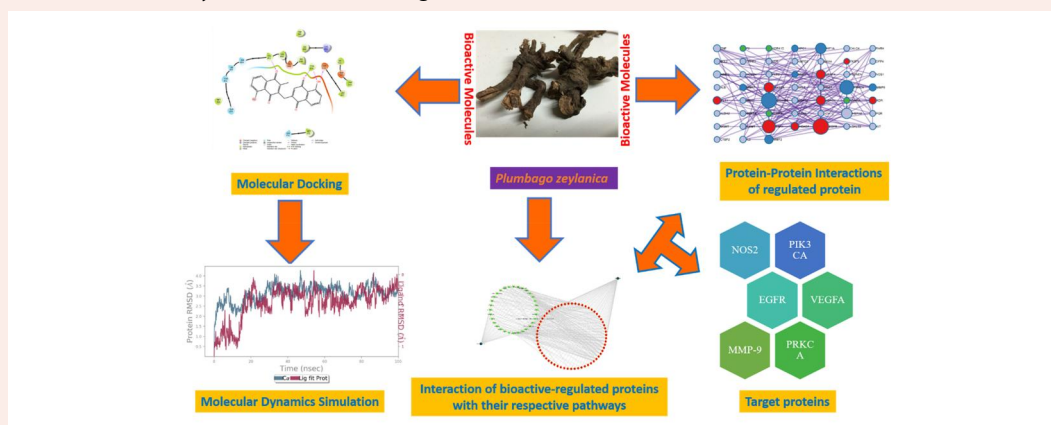
Plumbago zeylanica is an important plant used in the Ayurvedic system of medicine for the treatment of hemorrhoids or piles. Despite its clinical uses, its molecular mechanism, for ameliorating hemorrhoids is not yet explored. Hence, the present study evaluated the plausible molecular mechanisms of *P. zeylanica* in the treatment of hemorrhoids using network pharmacology and other in silico analysis. Network pharmacology was carried out by protein, GO, and KEGG enrichment analysis. Further ADME/T, molecular docking and dynamics studies of the resultant bioactive compounds of *P. zeylanica* with the regulated proteins were evaluated. Results of the network pharmacology analysis revealed that the key pathways and plausible molecular mechanisms involved in the treatment effects of *P. zeylanica* on hemorrhoids are cell migration, proliferation, motility, and apoptosis which are synchronized by cancer, focal adhesion, and by signalling relaxin, Rap1, and calcium pathways which indicates the involvement of angiogenesis and vasodilation which are the characteristic features of hemorrhoids. Further, the molecular docking and dynamics studies revealed that the bio active ingredients of *P. zeylanica* strongly bind with the key target proteins in the ambiance of hemorrhoids. Hence, the study revealed the mechanism of *P. zeylanica* in ameliorating hemorrhoids.

ARTICLE HISTORY

Received 2 August 2023
Accepted 1 November 2023

KEYWORDS

Ayurveda; GO analysis; KEGG pathway; molecular docking; piles



HIGHLIGHTS

- Potential mechanisms of treatment of hemorrhoids are related to the processes including cell migration, regulation of cell population proliferation, cell motility, and apoptosis.
- The molecular docking outcomes reveal that the active ingredients of *P. zeylanica* bind with the key target proteins, such as PIK3CA, EGFR, PRKCA, VEGFA, MMP-9 and NOS2 in the management of hemorrhoids.
- Altogether, this study unveils the systemic biological profiles of *P. zeylanica*.

1. Introduction

Hemorrhoids (Piles) are inflamed veins that have undergone excessive swelling and inflammation which mainly arises around the anorectal region. The formation of hemorrhoids

usually occurs because of elevated pressure in the veins in the anorectal region which dilate and distort the vascular channel abnormally leading to extravasation in the blood vessels resulting in bleeding. Epidemiological studies

suggests the prevalence rate of hemorrhoids is 11% (Sheikh et al., 2020). Treatment of hemorrhoids includes lifestyle modification, drug therapy, sclerotherapy, and surgery. The exact cause and development of hemorrhoids have not yet been fully explained due to the complexity of its origins and pathogenesis. The phenomenon and the headway of hemorrhoids are mainly related to five reasons i.e. constipation, relaxation of supportive tissue in the rectal area, increased pressure in the abdominal region, reduced venous return during defecation, and blood stagnation inside the dilated plexus (Margetis, 2019). The mechanisms of the currently commercially available anti-hemorrhoidal drugs are based on palliative treatment. Because of the limited available therapeutic agents for treating hemorrhoids, the traditional system of medicines is the only available therapy that needs to be developed and explored. However, very few studies delineated the experimental evaluation of medicinal plants on hemorrhoids. Therefore, the development and utilization of new anti-hemorrhoidal drugs are inescapable.

Plumbago zeylanica L (family Plumbaginaceae), popularly well-known as *chitraka*, *chita*, *chitra* and *chitra-moolam*. The roots and root barks have high medicinal uses such as they are bitter, stomachic, carminative, anthelmintic, astringent, curing intestinal troubles, dysentery, inflammation, piles, bronchitis, constipation, rheumatic diseases, and skin diseases. *P. zeylanica* roots are widely used in the Ayurvedic system of Medicine for the treatment of *Arsa* (piles), *Sotha* (inflammatory disease), *Grahani* Roga (disorders in the intestine), *Udarsula* (abdominal pain), and *Gudasotha* (inflammation of the rectum) (Chowdhury et al., 2020; Edition, 2016; Madan et al., 2023; Patel et al., 2021; Satyavati et al., 1987; Sharma et al., 2000). Previous studies reported that the root extracts exhibited CNS stimulatory, hypolipidemic, anti-tumor, antimicrobial, anticancer, and wound healing activities (Dwivedi, 1997; Makhal et al., 2021; Parveen et al., 2023; Shrimali et al., 2001). The major phytoconstituents of the root include plumbagin, 3-chloroplumbagin, elliptinone, chitranone, isozeylanone, 2-(1-hydroxy-1-methyl-ethyl)-9-methoxy-1,8-dioxo-dicyclopenta-b-g-Naphthalene-4,10-dione, droserone, zeylenone, plumbagic acid, plumbazeylinone, naphthalenone and isoshinanolone (Lin et al., 2003; Nandi, Das, Lin, & Chakraborty, n.d.; Sidhu & Sankaram, 1971). Despite of the traditional and Ayurvedic use of *P. zeylanica* in hemorrhoids, no studies have scientifically evaluated its mechanism for ameliorating hemorrhoids. Hence, in this study, we first introduced network pharmacology to analyze the phytoconstituents and signaling pathways of the anti hemorrhoidal effect of the *P. zeylanica*. This network pharmacology study revealed the synergistic effect of various phytoconstituents and their mechanisms through the various targets for the treatment of hemorrhoids.

2. Materials and methods

2.1. Identification of bioactive compounds and targets

In this study, phytoconstituents were obtained from the IMPPAT (Indian Medicinal Plants, Phytochemistry, and

Therapeutics) database (<https://cb.imsc.res.in/imppat/>) and PubMed (<https://pubmed.ncbi.nlm.nih.gov/>). The PubChem database (<https://pubchem.ncbi.nlm.nih.gov/>) was used to collect additional information, including PubChem ID, CAS, canonical smiles, and 2D structures of the phytoconstituents. To predict the targets of the phytoconstituents, two web servers, BindingDB (<https://www.bindingdb.org/bind/index.jsp>) and Swiss Target Prediction (<http://www.swisstargetprediction.ch/>), were utilized. These servers are based on the bioactive compounds of *P. zeylanica* and their probable targets. For identifying hemorrhoid-specific targets, data were derived from the DisGeNET database (<https://www.disgenet.org/>), the GeneCards database (<https://www.genecards.org/>), and the OMIM webserver (<https://www.omim.org/>). The keyword 'Hemorrhoids' and the organism 'Homo sapiens' were used to search for relevant targets. The identified targets were verified using UniProt ID, and their names were standardized into official gene symbols with the help of the UniProt database (<https://www.uniprot.org/>). The Venn diagram created using Venny2.1.0 (<https://bioinfo.gp.cnb.csic.es/tools/venny/index.html>) was employed to find the mutual targets shared between the bioactive constituents and hemorrhoids.

2.2. Collection of protein-protein interaction (PPI) data

The selected targets were integrated into the STRING11.0 database (<https://string-db.org/>) to construct a PPI network, focusing on 'Homo sapiens' as the species and setting a minimum interaction threshold of 'high confidence > 0.7'. To improve clarity, detached nodes were concealed in the network visualization using Cytoscape software. To identify highly interconnected clusters within the PPI network, we employed the Molecular Complex Detection (MCODE) algorithm (version 1.5.1), a Cytoscape plug-in. We applied specific threshold parameters: a maximum depth of 100, a node score of 0.2, and a K-core of 2 (M. Zhang et al., 2021) to facilitate the identification of PPI sub-networks.

2.3. GO and KEGG enrichment analyses

To predict the Gene Ontology (GO) biological processes, we utilized ShinyGO 0.76, and for enrichment analyses, we employed the Kyoto Encyclopedia of Genes and Genomes (KEGG) metabolic pathway analysis, focusing on the mutual targets of *P. zeylanica* and hemorrhoids. The top 20 biological pathways and processes were selected based on a False Discovery Rate cutoff of 0.05 and fold enrichment. These results were presented as bubble charts, showing adjusted *p*value, fold enrichment, and gene counts. The GO analysis provided insights into various biological processes, cellular components, and molecular functions. To discover key target proteins crucial for the treatment effects of *P. zeylanica*, we constructed a network using the significant pathways obtained from the KEGG analysis (Song et al., 2022). All the information regarding the key targets and involved pathways was obtained from online software, aiding

in predicting the likely mechanism of action of the bioactive ingredients of *P. zeylanica* in the treatment of hemorrhoids.

2.4. Molecular docking validation

The phytoconstituents used in this study were obtained from publicly accessible databases. Molecular docking studies were conducted on the 32 compounds which were screened from 37 compounds using Glide XP from Schrödinger 2017_2. The ligands' energy-minimized structures were docked with the crystal structures of human PIK3CA (PDB ID: 7JIU, resolution of 2.12 Å), EGFR (PDB ID: 3W2S, resolution of 1.90 Å), vascular endothelial growth factor (VEGF) (PDB ID: 1VPP, resolution of 1.90 Å), matrix metalloproteinase 9 (PDB ID: 5CUH, resolution of 1.83 Å), nitric oxide synthase (PDB ID: 3E7G, resolution of 2.20 Å), and the predicted structure of PRKCA (Gene: Prkar1a) using the AlphaFold algorithm, with validated grid parameters (Abdizadeh et al., 2020; Chattaraj et al., 2023; Chattaraj et al., 2022; Hong et al., 2021).

2.5. Molecular dynamics validation

The protein-ligand complexes obtained from docking were subjected to simulation using the Desmond module within the Schrödinger software. An orthorhombic box was constructed using the system builder panel. For the simulation of the docked ligand-protein complex, a simple point charge model was employed as the water model. The molecular dynamics (MD) simulation was performed using the constant-temperature, constant-pressure ensemble (NPT) at 310 K and 1.013 bar, representing atmospheric pressure, for a duration of 100 ns. The results of the molecular dynamics studies were thoroughly analyzed using the Simulation Interactions Diagram Report available in the Desmond software (Auti et al., 2022; Bowers et al., 2006; Chattaraj et al., 2023; Nandi et al., 2023; Wang et al., 2019).

2.6. Induced fit docking (IFD)

The Induced Fit Docking (IFD) process was conducted on the most promising bioactive compounds with their respective receptors as follows: isozeylanone with PIK3CA [7JIU], isozeylanone with EGFR [3W2S], zeylanone with PRKCA ((Gene: PRKACA) (AlphaFold)), methylnaphthazarin with VEGFA [1VPP], zeylanone with MMP-9 [5CUH], and isozeylanone with NOS2 [3E7G]. The Schrödinger software 2017-2's Induced Fit Docking panel was utilized for this purpose, and the protocol's details were described in a previous study (Tutone et al., 2019). Between the standard and extended sampling protocols, the former was chosen, which produced up to twenty docked poses using automatic docking settings and utilized the OPLS3 force field for IFD calculations. The best poses generated from the initial Glide XP docking of bioactive compounds with their respective receptors were used as input structures for IFD. The centroid of the ligands was selected to generate the grid box, and no additional constraints were applied. A ring-conformational sampling of the ligands was performed within a 2.5 kcal/mol energy

window. The initial Glide docking was carried out by setting both the receptor and ligand's van der Waals scaling to 0.5. Subsequently, the amino acid residues within 5 Å of the ligand were refined using the Prime module of Schrödinger. Afterward, the Prime-refined receptor-ligand complexes within a 30 kcal/mol energy range were redocked using the Glide XP mode, while other parameters remained at their default values.

2.7. MM-GBSA calculation

The binding free energy was determined using the molecular mechanics-generalized Born surface area (MM-GBSA) method, which combines solvent accessibility, molecular mechanics, and the generalized Born model to avoid convolution in free energy simulations (Genheden & Ryde, 2015). The energy difference between the bound and unbound states of the protein-ligand complex was calculated using MM-GBSA. The binding free energies were computed using the following equation:

$$\text{MM-GBSA } \Delta G_{\text{Bind}} = G_{\text{Complex}} - (G_{\text{Receptor}} + G_{\text{Ligand}}).$$

Here the MM-GBSA calculation was done in Prime software [(Jacobson et al., 2004)9] by considering the VSGB solvation model with OPLS3 Force Field with minimized sampling method.

2.8. In silico physicochemical and ADME/T studies

Qikprop module of Schrödinger suite 2017-2 (QikProp | Schrödinger, n.d.) and SwissADME (Daina et al., 2017) web-server was used to determine the physicochemical and ADME/T properties of the best three molecules which helps to determine the physicochemical significant descriptors and pharmacokinetically important properties of the molecules. For the toxicity prediction of the best three molecules, ProTox-II webserver (https://tox-new.charite.de/prottox_II/index.php?site=compound_search_similarity) was used.

3. Results and discussion

Hemorrhoids are the swollen and inflamed veins around the anoctal tissue which are assumed to be formed due to erosion of the protective connective tissue resulting in vasodilation and extravasation in the inflamed region. Because of the limited available therapeutic agents for treating hemorrhoids, the traditional system of medicines is the only available therapy that needs to be developed and explored. *P. zeylanica* is one of the medicinal plant mentioned in Ayurvedic System of Medicine as an antihemorrhoidal agent which consist of many phytoconstituents. In view of the traditional use of *P. zeylanica* in hemorrhoids, the present study determined the potential mechanisms for the antihemorrhoidal effects of *P. zeylanica* through network pharmacology approaches. Results indicated that many proteins related to the different biological processes and signalling pathways can be targeted by the bioactives of *P. zeylanica* to alleviate hemorrhoidal conditions.

3.1. Identification of bioactive compounds and targets

A total of 37 bioactive phytoconstituents were obtained from the IMPPAT database through a keyword search for '*Plumbago zeylanica*'. Using the BindingDB (Supplementary Table S1) and SwissTargetPrediction (Supplementary Table S2) databases, a total of 781 targets for the various phytoconstituents of *P. zeylanica* were identified. Additionally, 24, 579, and 1 hemorrhoid-related targets were predicted from three different databases: DisGeNET database (Supplementary Table S3), GeneCards (Supplementary Table S4), and OMIM (Supplementary Table S5), respectively. By removing repetitive gene symbols, a total of 597 unique hemorrhoid-related targets were obtained from these databases (Supplementary Table S7). The common targets between the phytoconstituents and hemorrhoid-related targets were compiled in Supplementary Table S6. A total of 58 common targets (Supplementary Table S8) were identified through the intersection of *P. zeylanica*-derived bioactive targets and hemorrhoid targets (Figure 1A). Upon analyzing the common targets, it was confirmed that 32 phytoconstituents of *P. zeylanica* are involved in the treatment of hemorrhoids. Detailed information about these active ingredients is available in Supplementary Table S9.

3.2. Common targets and PPI network analysis

The active ingredients and common targets were introduced into Cytoscape 3.9.1 for constructing a network Figure 1B and Supplementary Figure 1 among them, where 32 bioactive compounds and 58 common targets, and their 341 edges were visible, with high confidence (0.70) and the PPI enrichment *p*value of $< 1.0e^{-16}$. This constructed network indicated the occurrence of numerous and complex effects of the bioactive constituents of *P. zeylanica* phytoconstituents on hemorrhoids. The proteins have a large number of interaction among each other as expected. Based on the gradation, the utmost common targets were mentioned in a column chart

(Supplementary Table S10). Results revealed that the most prominent hemorrhoids-associated genes were CTNBN1, TNF, ALB, VEGFA, EGFR, ESR1, HIF1A, MMPs, ICAM1, KDR, KIT, IL2, PRKCA, SELE, HDAC1, LGALS3, PGR, FLT1, PIK3CA, NOS2 due to treatment of *P. zeylanica* (Supplementary Table S11). The results of the MCODE also suggests the significance of the above mentioned genes in the proteins (Supplementary Figure 2A and B). In the network (Figure 2A), the 32 phytoconstituents and all the 58 common targets were clearly revealed. In extent, we applied Cytohubba plug-in for the investigation of topological network of the top 20 nodes of the common genes (Figure 2B). This enrichment analysis indicates that the proteins are at least partially biologically connected, as a group. We selected the nodes with more than twice the median edge count of all nodes to construct the hub PPI.

3.3. GO and KEGG enrichment analyses

The results of the GO analysis revealed that *P. zeylanica* bioactives primarily target the response to inflammation by promoting increased proliferation and infiltration of inflammatory cells and apoptosis. In GO enrichment study, the results revealed the multidimensional and complex effect of *P. zeylanica* and discovered various biological processes which are related to hemorrhoids, such as cell migration, regulation of cell population proliferation, cell motility, and regulation of programmed cell death terms.

In the KEGG pathway enrichment analysis, a total of 151 signaling pathways were found to be mainly involved in the interactions of *P. zeylanica* bioactive constituents in ameliorating hemorrhoids. Out of them, the top 20 pathways were depicted in Supplementary Figures S3–S8, sorted by the number of genes involved in the expressed pathways. The main pathways that were expressed included pathways in cancer, relaxin signaling pathways, focal adhesion, Rap1

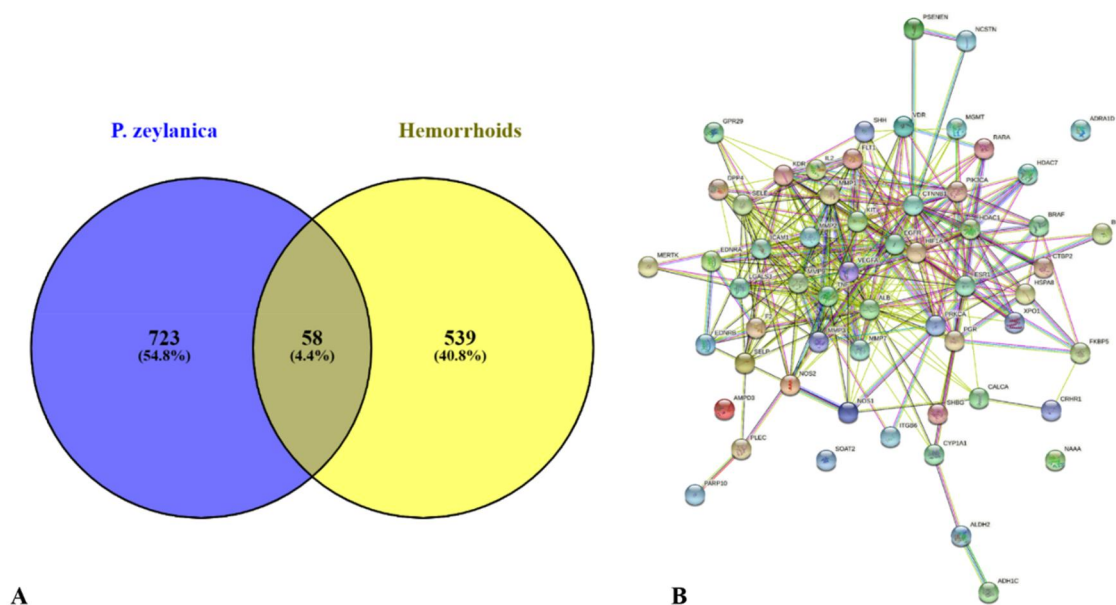


Figure 1. Screening of *P. zeylanica*-hemorrhoids common targets and PPI analysis. (A) Venn diagram of *P. zeylanica*-hemorrhoids common targets. (B) PPI network of common targets originated from STRING.

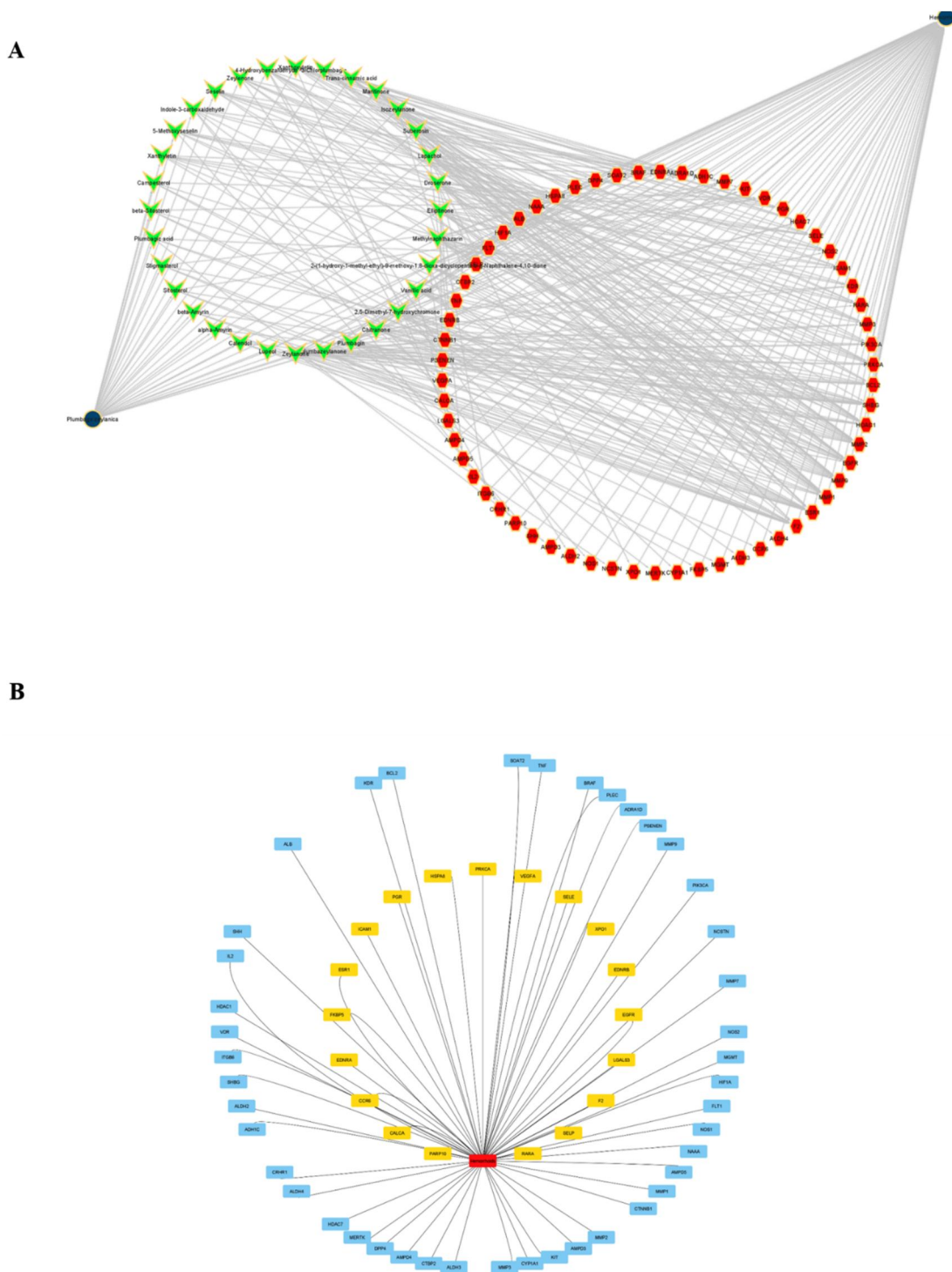


Figure 2. Active ingredient-hemorrhoids target network. (A) The active ingredients of *P. zeylanica* (32 phytoconstituents) and the common targets (58 targets). (B) The top 20 nodes visualised in Cytoscape calculated by Cytohubba.

signaling pathway, and calcium signaling pathway, all of which are closely associated with angiogenesis and extravasation processes, characteristic features of hemorrhoids. Through this study, significant key targets of *P. zeylanica* bioactives responsible for the pathogenesis of hemorrhoids were identified by selecting the top 10 signaling pathways (Table 1) based on the number of genes involved. Furthermore, the common target genes involved in ameliorating hemorrhoids through various phytoconstituents of *P.*

zeylanica were found to be VEGFA, EGFR, MMP-9, PIK3CA, and PRKCA, which are also known to play crucial roles in the pathogenesis of hemorrhoids.

The results of the PPI network and GO analysis showed that the *P. zeylanica*-hemorrhoids common targets were mainly the key proteins involving the pathways: inflammation (ALB), cell adhesion (CTNNB1, SELE, LGALS3, and ICAM1), cytokines (TNF, IL-2), angiogenesis (VEGFA, EGFR, HIF1A, PRKCA, PIK3CA, KDR, FLT1, MMPs), vasodilation (NOS2),

Table 1. Targets genes involved in the top 10 signaling pathways.

Pathway	Target genes
Pathways in cancer	NOS2, MMP2, ESR1, HIF1A, MMP9, IL2, VEGFA, HDAC1, PIK3CA, RARA, EDNRB, EGFR, EDNRA, PRKCA, KIT, BRAF, SHH, CTNNB1, BCL2, CTB2, F2, MMP1
Proteoglycans in cancer	MMP2, ESR1, HIF1A, MMP9, VEGFA, PIK3CA, KDR, EGFR, PRKCA, BRAF, SHH, CTNNB1, TNF
Lipid and atherosclerosis	SELE, ICAM1, MMP9, HSPA8, PIK3CA, CYP1A1, MMP3, PRKCA, BCL2, SELP, MMP1, TNF
Estrogen signalling pathway	PGR, MMP2, ESR1, FKBP5, MMP9, HSPA8, PIK3CA, RARA, EGFR, BCL2
Relaxin signalling pathway	NOS2, MMP2, NOS1, MMP9, VEGFA, PIK3CA, EDNRB, EGFR, PRKCA, MMP1
Focal adhesion	FLT1, VEGFA, ITGB6, PIK3CA, KDR, EGFR, PRKCA, BRAF, CTNNB1, BCL2
Fluid shear stress and atherosclerosis	SELE, MMP2, ICAM1, MMP9, VEGFA, PIK3CA, KDR, CTNNB1, BCL2, TNF
Calcium signalling pathway	NOS2, NOS1, FLT1, VEGFA, KDR, EDNRB, EGFR, EDNRA, PRKCA, ADRAID
Coronavirus disease	IL2, PIK3CA, EGFR, MMP3, PRKCA, SELP, F2, MMP1, TNF
Rap1 signalling pathway	FLT1, VEGFA, PIK3CA, KDR, EGFR, PRKCA, KIT, BRAF, CTNNB1

estrogen release (ESR1, PGR), and cell proliferation (KIT, HDAC1). In hemorrhoids, an inflammatory response due to the anorectal tissue damage and the blood vessel endothelial cells distortion cause the formation of ulcers in the rectal mucosa and thrombosis (Lohsiriwat, 2012) and reduces the level of albumin. It also causes the migration of various inflammatory cells like T-lymphocytes, macrophages and neutrophils, etc. which secretes various anti-inflammatory cytokines and chemokines (Porwal et al., 2021; Shrivastava et al., 2018) which sticks in the inflammatory region through cell adhesion molecules (CTNNB1, SELE, LGALS3, and ICAM1). IL-1 β , IL-2, IL-6, VEGF and TNF- α are known to be important inflammatory markers during the progression of inflammation (Gulati et al., 2016; Wojdasiewicz et al., 2014) such as in hemorrhoids. In the present study, the results showed that the various cytokines were the target proteins of *P. zeylanica*. Previous studies revealed that the bioactives of *P. zeylanica* caused the inhibition of the migration of T cells in the affected area by arresting the cell cycle which resulted in decreased secretions of various cytokines (Checker et al., 2009) which supports the current findings. The vascularization around the hemorrhoidal tissue usually profoundly increase indicating the aggravation of angiogenesis around the hemorrhoidal tissue which cause the increase in the concentrations of growth factors like VEGF or Fms Related Receptor Tyrosine Kinase 1 (FLT1) and endothelial growth factor through their receptors (EGFR), Hypoxia induced factor (HIF1A), Kinase Insert Domain Receptor (KDR) (Chung et al., 2004; Han et al., 2005). The signalling pathways mediated by these growth factors are prominently involved in the development of haemorrhoids (Liu et al., 2021; Van Crujisen et al., 2005). Due to the anorectal tissue damage in hemorrhoids, an important enzyme i.e. matrix metalloproteinase causes the degradation and erosion of the upper protective connective tissue like elastin. The most potent matrix metalloproteinase responsible for the occurrence of hemorrhoids is MMP-9 which damages the elastic fibres (Han et al., 2005) and enhance the angiogenesis process. Protein kinase C alpha (PRKCA) is also known to promote angiogenic activity of human endothelial cells via induction of VEGF (H. Xu et al., 2008). Protein kinase C (PIK3CA AND KIT gene) (Kobialka et al., 2022) and Histone deacetylase 1 (HDAC1) also activates the mutation in endothelial cells which triggers a transcriptome rewiring that leads to enhanced cell proliferation and produce vascular malformations. Previous studies revealed that the bioactives of *P. zeylanica* inhibited the

anti-angiogenic factors in experimental studies (Hafeez et al., 2013) which supports the current findings and highlights the anti-angiogenic role of *P. zeylanica* which may be responsible for the amelioration of hemorrhoids. The distortion of blood vessels cause the formation of endothelial derived relaxin factors like NO which is catalysed by NO synthase (NOS2) resulting in vasodilation and extravasation, a characteristics feature in hemorrhoids. The present study revealed that the phytoconstituents of *P. zeylanica* have a prominent role in regulating NOS2 which suggests the preventive role of the plant in extravasation and edema in hemorrhoids. Previous reports suggest estrogen and progesterone are responsible for formation of edema through the estrogen receptors (ESR1), progesterone receptors (PGR) in the anorectal region causing the severity of hemorrhoids which is reversed by anti-estrogenic drugs (Meng et al., 2022). The present study revealed that the phytoconstituents have regulated ESR1 and PGR reflecting the anti-estrogenic property of this phytoconstituents that may attenuate hemorrhoidal symptoms. The previous experimental results showed that *P. zeylanica* extracts have the anti-estrogenic property which supports our current findings (Sandeep et al., 2011). The results showed that the PRKCA, PIK3CA, MMP-9 and VEGFA and EGFR were the target proteins of *P. zeylanica*. Based on the findings of network pharmacology the hypothetical mechanisms of the bioactive phytoconstituents of *P. zeylanica* in amelioration of hemorrhoids is depicted in Figure 3.

3.4. Molecular docking validation

Based on the results of KEGG enrichment analysis, we examined the involvement of various expressed pathways in the occurrence of hemorrhoids. These pathways include pathways in cancer (associated with angiogenesis in tumors/cancer), relaxin signaling pathways (related to vasodilation and extravasation), focal adhesion (implicated in cytokine migration through adhesion molecules), Rap1 signaling pathway (playing a role in signal transduction), and calcium signaling pathway (having a role in signal transduction and vasoconstriction). Furthermore, we investigated several genes that may be highly relevant to the incidence of hemorrhoids. These genes, including PIK3CA (nine times), EGFR (eight times), VEGFA (seven times), MMP-9 (six times), PRKCA (eight times), and NOS2 (three times), were enriched in the top ten pathways in the KEGG enrichment analysis. PPI analysis indicated that these pathways are crucial targets for hemorrhoids. To validate the

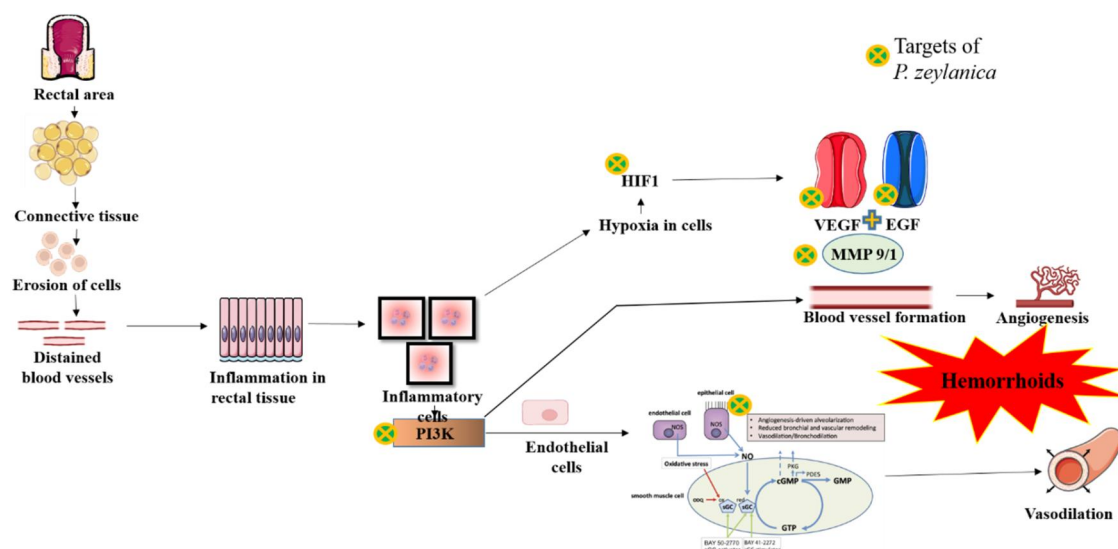


Figure 3. Schematic diagram of important pathways and key targets of *P. zeylanica* in the treatment of hemorrhoids. The proteins labelled with small green circle are target proteins of *P. zeylanica*. Some intermediate pathway-related molecules are omitted.

network pharmacology results, we performed molecular docking on the active ingredients and these six key targets. Molecular docking is a widely used method to explore molecular interactions between protein targets and small molecules. Scientists commonly use this approach to identify the active sites and binding residue details. The Glide XP docking scores and the amino acid residues responsible for the interactions are listed in (Supplementary Table S12 and Supplementary Table S13, respectively). Based on the docking scores, we analyzed the 3D and 2D interaction diagrams of the top three compounds to understand their proposed activity (Figure 4; Supplementary Figures S9–S11). Docking studies has been done in duplicate for the data reliability. Negative binding energy indicates the effective binding to the target. Lower binding energy suggested stable ligand-receptor complex better explained as <-5 kcal/mol called as good binding activity and <-7 kcal/mol called as strong binding activity.

The top three compounds based on GlideScore against the PIK3CA (PDB ID: 7JIU) were found to be isozeylanone (-10.467 Kcal/mol), 2-(1-hydroxy-1-methyl-ethyl)-9-methoxy-1,8-dioxo-dicyclopenta-b-g-Naphthalene-4,10-dione (-10.307 Kcal/mol), and 3-chlorplumbagin (-9.135 Kcal/mol). All the compounds have the optimum interactions with the active site (Methot et al., 2020). The result indicated Val 851 is the most common amino acid responsible for the H-bond formation whereas Met 772, Trp 780, Ile 800, Tyr 836, Ile 848, Val 850, Val 851, Met 922, and Ile 932 were the binding residue responsible for strong hydrophobic interactions in the binding pocket. However, Ser 854 was able to form Polar interaction in all the cases (Supplementary Figure S9A, Supplementary Figure S12A).

In the active site (Sogabe et al., 2013) of EGFR (PDB ID: 3W2S) the top three compounds based on GlideScore were found to be isozeylanone (-11.511 Kcal/mol), chitrone (-10.200 Kcal/mol), and zeylenone (-8.353 Kcal/mol). The amino acid Met 793, Thr 854, and Thr 790 were accountable for H-bond formation and Polar interaction respectively. Leu 777 and Leu 788 were the most common amino acids

behind the hydrophobic interactions ((Supplementary Figures S9B and S12B)).

However, in PRKCA (Gene: PRKACA) (AlphaFold)), zeylenone (-7.905 Kcal/mol), suberosin (-6.941 Kcal/mol), and 4-Hydroxybenzaldehyde (-6.264 Kcal/mol) were found to be more potent. Leu 50, Val 58, Ala 71, Val 105, Met 121, Tyr 123, Val 124, Leu 174, and Phe 328 were the most common amino acids responsible for the hydrophobic interactions and Thr 184 was for polar interaction (Supplementary Figures S10A and S12C) present in the binding site (SiteMap-predicted, Schrödinger Inc.).

In VEGFA (PDB ID: 1VPP), methylnaphthazarin (-5.193 Kcal/mol), plumbagic acid (-4.821 Kcal/mol), and maritinone (-4.491 Kcal/mol) were the top three compounds based on molecular docking results. Arg 82, Tyr 45, and His 90 were the common amino acids present in the binding site (SiteMap-predicted, Schrödinger Inc.) which were responsible for the H-bond formation, hydrophobic interactions, and polar interaction, respectively (Supplementary Figures S10B and S12D).

In the active site (Camodeca et al., 2016) of MMP9 (PDB ID: 5CUH), zeylenone (-8.670 Kcal/mol), isozeylanone (-7.801 Kcal/mol), and 2-(1-hydroxy-1-methyl-ethyl)-9-methoxy-1,8-dioxo-dicyclopenta-b-g-Naphthalene-4,10-dione (-7.388 Kcal/mol) have the common H-bond interactions with the Met 247. Whereas the Leu 222, Val 223, Ala 242, Leu 243, Tyr 245, Pro 246, Met 247, Tyr 248, and Pro 255 were the responsible amino acids that helped in the hydrophobic interactions while His 226, Hie 236, and Thr 251 were responsible for the polar interactions in the binding pocket (Supplementary Figures S11A and S12E).

In the active site (Garcin et al., 2008) of NOS2 (PDB ID: 3E7G) Trp 194, Ala 197, Val 352, Phe 369, Trp 463, Tyr 489, and Tyr 491 were the amino acids that are responsible for the hydrophobic interactions. On the other hand Asn 370 was the common amino acids for polar interactions (Supplementary Figures S11B and S12F).

Except the VEGFA all the GlideScore of the top three compounds against the other five proteins were in the range of

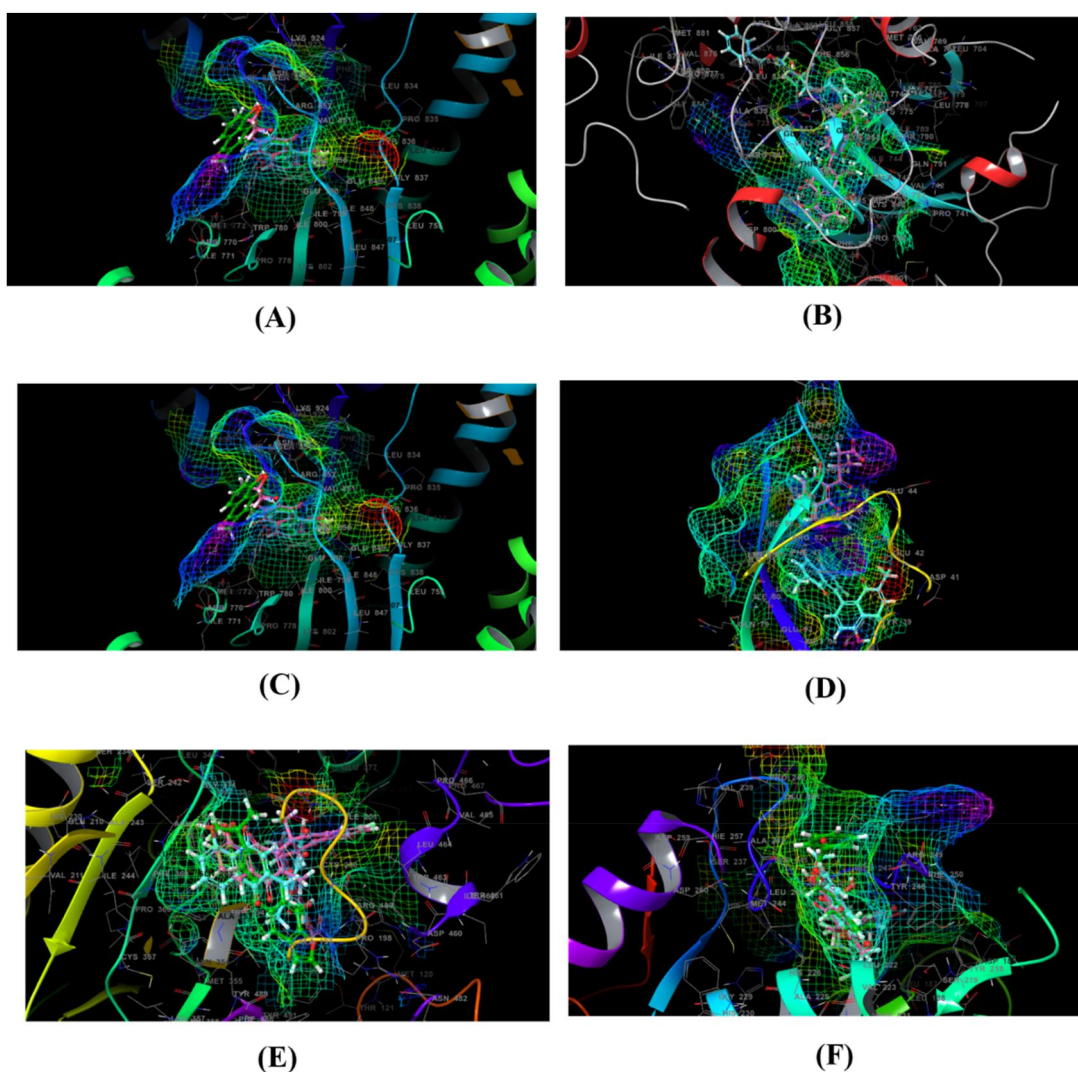


Figure 4. Molecular docking results (superimposition of the best active ingredients) of key targets i.e PIK3CA (a), EGFR (B), PRKCA (C), VEGFA (D), MMP9 (E), and NOS2 (F) and specific active ingredients of *P. zeylanica*.

–11.511 to –6.264 kcal/mol. The top three active ingredients for the above-mentioned proteins were evinced to have a strong binding interaction with their respective proteins. It involves unforeseeable bias from the materiality, which could expedite to anonymous fallacy in *in-vitro* or *in-vivo* studies. However, this molecular docking outcomes throwback plausible treatment mechanisms and it may direct the animal affirmation experiment.

Previous literature suggests that zeaylenone has shown promising effect in mitigating inflammation and combating cancer. In a study by Yang et al. (Yang et al., 2021), it was shown to enhance the effects of cisplatin in osteosarcoma, leading to increased DNA damage, apoptosis, and necrosis through the Hsp90/AKT/GSK3 β and Fanconi anaemia pathway. Additionally, in ovarian carcinoma cells, Xu et al. (X. Xu et al., 2018) discovered that zeaylenone inhibits proliferation and induces apoptosis *via* the Janus kinase 2/signal transducers and activators of transcription 3 pathways. Moreover, zeaylenone exhibits antitumor effects in gastric cancer by inducing mitochondrial apoptosis and suppressing migration and invasion (Sun et al., 2021; Yang et al., 2018). It has also

demonstrated the ability to inhibit proliferation and induce apoptosis in cervical carcinoma cells through the PI3K/AKT/mTOR and MAPK/ERK pathways (L. Zhang et al., 2017). Furthermore, zeaylenone has been explored for its potential therapeutic effects in prostate cancer. Zeng et al. (Zeng et al., 2018) showed that zeaylenone hinders the progression of human prostate cancer by downregulating the Wnt/ β -catenin pathway. Isolated from *Uvaria grandiflora*, zeaylenone displays a wide range of promising biological activities, including fungicidal, anticancer, and anti-inflammatory effects (Cheng et al., 2023). Treatment with zeaylenone led to a decrease in the mRNA expression of pro-inflammatory factors IFN- γ , iNOS, IL-6, and TNF- α by downregulating the NF- κ B signaling pathway. Hence, the reported anti-inflammatory role of zeaylenone supports our current findings.

3.5. Molecular dynamics

In computer aided drug designing the molecular dynamics simulations of the protein-ligand complexes are considered

as the most mature technique in terms of the evaluation of the macromolecular structure to-function correlation. In this current study the impartial molecular dynamics study was performed to demystify the firmness of the ingredients of *P. zeylanica* against the six proteins akin to the hemorrhoids. With the generation of 100 ns MD simulations the root mean square deviation (RMSD), the root mean square fluctuation (RMSF), protein-ligand contacts were generated and carefully analysed their significance in the solidity of the protein-ligand complexes. Molecular dynamics studies have been done in duplicate for the data reliability.

3.5.1. Stability analysis

For the evaluation of dynamic stability of the protein-ligand complexes the RMSD was selected as a criterion. We decided to analyse the best docking pose of the top dock scoring active ingredients of each of six proteins in terms of binding interactions. All the queried protein frames were aligned against the reference frame to check the median replacement of atoms, in this cases $C\alpha$. In the case of small, globular proteins the replacement of $<3\text{ \AA}$ in RMSD evolution (left Y-axis) is acceptable. Ligand RMSD clearly stipulate the stability of the ligand concerning the protein and its binding site. Here the 'Lig fit Prot' revealed that the RMSD of a ligand when the protein-ligand complex was aligned first time on the mainstay of the reference protein and the RMSD of the heavy atoms were estimated. Nevertheless, the greater replacement stipulate higher conformational change during the simulation. The PIK3CA protein system outstretched to equilibrium briskly and swing around the average value of 1.5 \AA , the lower average value of ligand RMSD = 0.5 \AA which indicates brawny solidity of the isozeylanone in the binding site of PIK3CA after the $\sim 15\text{ ns}$. Probably this solidity is due to the presence of four aromatic ring, two hydroxyl group as well as four keto group (Figure 5A1). For the EGFR- isozeylanone complex, the RMSD values of protein's $C\alpha$ atoms and the ligand are reported in (Figure 5B1). The EGFR- isozeylanone complex, after 8-18 ns the RMSD value of $1-1.6\text{ \AA}$, reached the equilibrium sustaining the oscillation of $<1.0\text{ \AA}$. Both the protein and ligand were in a stable mode during the 100 ns simulations which indicates of a good binding interactions and also satisfy the best Glide Score of -11.511 Kcal/mol . The behaviour of the PRKCA-zeylenone was quite stable if compared to the previous one. The system reached equilibrium swiftly from the 0 ns and sustained stable oscillation along with the rest of the simulation period with an average RMSD of $<1.0\text{ \AA}$. This value was interesting considering the Glide Score of -7.905 Kcal/mol and demonstrating good stability of zeylenone in the binding site of PRKCA (Figure 5C1). For the complex of VEGFA-methylnaphthazarin the stability was not sustained and there was fluctuations throughout the 100 ns. But the protein RMSD as well as ligand RMSD for this complex was $<3\text{ \AA}$ if some certain peaks were ignored (Figure 5D1). Here in case of MMP9 the zeylenone molecule is showing good stability in the binding pocket of the protein. The system was in highly stable equilibrium except the 7-12 ns of the total simulation time. The MMP9-zeylenone complex RMSD were reported to be an

average of 1 \AA . Probably the absence of rotatable bond in the structure decrease the flexibility of the complex (Figure 5E1). The NOS2- isozeylanone complex is quite stable with a fluctuations of $<3\text{ \AA}$ (Figure 5F1).

3.5.2. Residue mobility analysis

The Root Mean Square Fluctuation (RMSF) typically represents the tails of the amino acids i.e. N and C- terminal which are able to fluctuate additionally than rest of the protein part. Alpha helices and beta strands are highly firm compared to its unstructured protein part. The residue wise fluctuations of the ligand-protein complexes are determined for the entire 100 ns simulation time. In case of PIK3CA- isozeylanone complexes the Arg 770-Met 922 amino acids region has the RMSF $<1.8\text{ \AA}$, which indicates the binding of the isozeylanone in the PIK3CA binding pocket is moderately influenced the protein (Supplementary Figure S13A1). EGFR- isozeylanone complex has the RMSF value of $<3.5\text{ \AA}$ in the Leu 718- Leu 1001 amino acid region (Supplementary Figure S13A2). The behaviour of the Leu 52- Phe 328 amino acids region of the PRKCA is slightly influenced with the RMSF $<0.8\text{ \AA}$ after the binding with zeylenone to its binding site (Supplementary Figure S13A3). Additionally RMSF $<2\text{ \AA}$ was observed for the Tyr 45-His 90 region of the VEGFA protein which indicates moderate influence of methylnaphthazarin in the binding pocket of VEGFA (Supplementary Figure S134). The MMP9- zeylenone complexes shows some acceptable RMSF (Supplementary Figure S13A5). Unlike the previous the Trp 194-Tyr 491 region of the NOS2 protein has the RMSF value of $<3.2\text{ \AA}$ with higher fluctuations after binding with isozeylanone (Supplementary Figure S13A6).

3.5.3. Protein-ligands contact analysis

Approximation of protein interactions provide a better picture of protein-ligand interaction and it is monitored throughout the 100 ns of the simulations. This protein-ligand interactions are categorized into four types: H-bonds, hydrophobic, ionic, and water bridges & the subtypes can be visualised through the 'Simulation Interactions Diagram' panel. The 0.4 value of the Y-axis of the stacked bar plot suggests that 40% of the simulation time the specific interaction is maintained.

Trp 780 (interaction fraction of 0.8; hydrophobic interactions), Val 851 (interaction fraction of 0.6; H-bond, interaction fraction of 1.5 water bridge), Ser 854 (interaction fraction of 0.25; H-bond, interaction fraction of 0.35 water bridge), and Ile 932 (interaction fraction of 0.4; hydrophobic interactions, interaction fraction of 0.1 water bridge), were the amino acids responsible for more protein-ligand contacts (proved by the intense orange colour of the protein-ligand contact). Ser 854 is responsible for the polar interaction. The visualization of ligand protein contact also revealed the possibility of intramolecular H-bond formation with the possibility of $>49\%$ (Figure 5A2, Supplementary Figure S13B1 and S13C1).

Lys 745 and Met 793 were the two amino acids for protein-ligand contacts of the EGFR- isozeylanone complex. Met 793 was able to form the hydrophobic bond as well as the

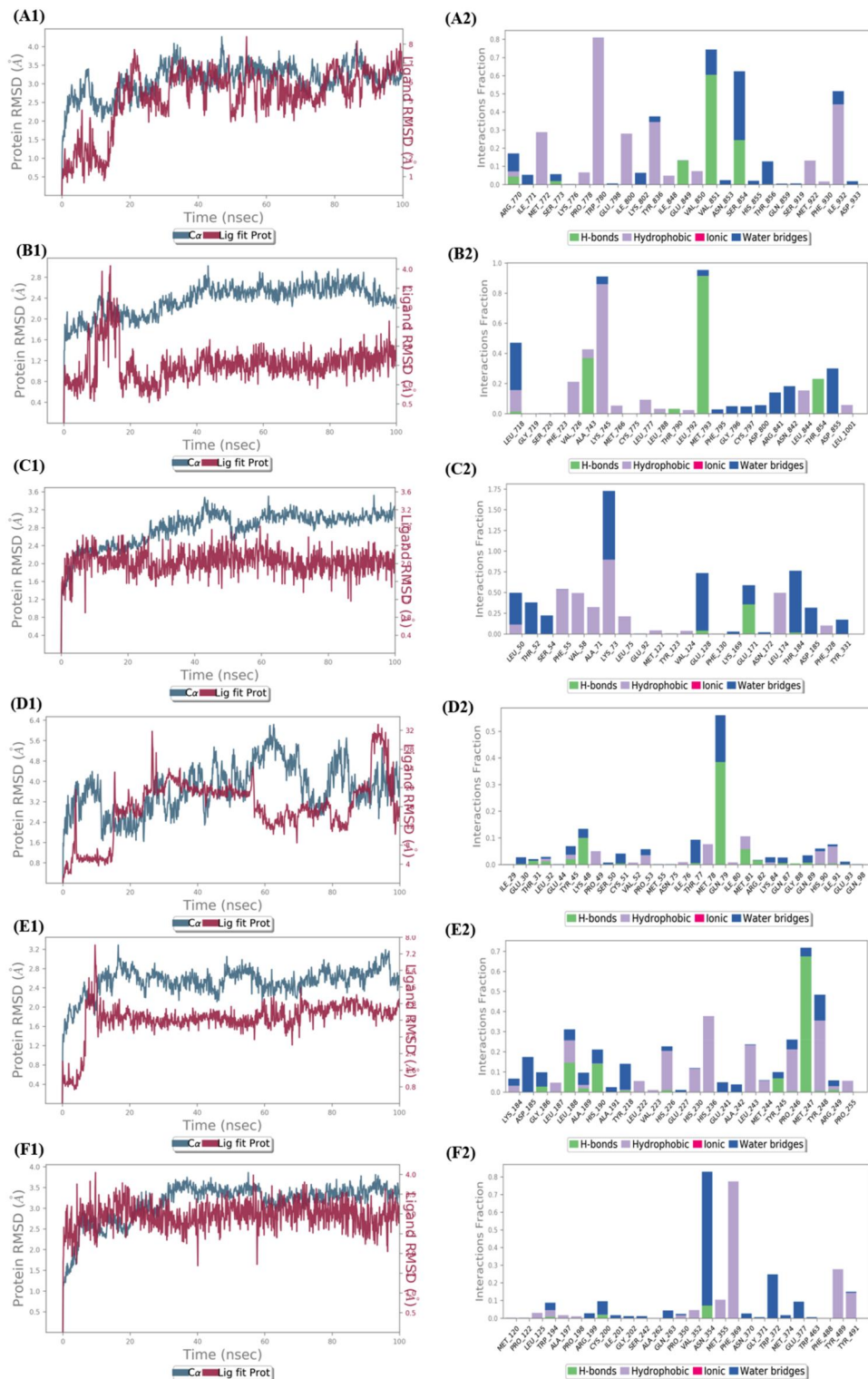


Figure 5. Molecular dynamics results of key target-ligands. 2D representation and Protein-Ligands contact analysis of PIK3CA-isozeylanone (A1, A2), EGFR-isozeylanone (B1, B2), PRKCA-zeylanone (C1, C2), VEGFA-methylnaphthazarin (D1, D2), MMP9-zeylanone (E1, E2), NOS2-isozeylanone (F1, F2) complexes.

H-bond for 91% of the simulation time in the selected trajectory with the keto group. Ala 743 and Lys 745 were another two amino acids responsible for the H-bond and hydrophobic interaction formation with the interaction fraction of 0.4 and 0.9 respectively (Figure 5B2, Supplementary Figure S13B2 and S13C2).

In case of the VEGFA- methylnaphthazarin, most important amino acid was Gln 79 with an interaction fraction of

0.3. This amino acid was highly responsible for the H-bond formation and other interactions (proved by the intense orange color of the protein-ligand contact). Pro 49, Met 78, Met 81, and Ile 91 were responsible for the strong hydrophobic interactions (Figure 5C2, Supplementary Figure S13B3 and S13C3).

The visualization of ligand protein contact also reveals the possibility of intramolecular H-bond formation with the

possibility of >67%. Additionally PRKCA-zeilynone complexes are stabilised Lys 73 (interaction fraction of 0.77; hydrophobic interactions, interaction fraction of 0.96; water bridge formation), Glu 128 (interaction fraction of 0.6; water bridge formation), Glu 171 (interaction fraction of 0.4; H-bond), and Thr 184 (interaction fraction of 0.6; water bridges). Leu 50, Phe 55, Val 58, Ala 71, Leu 75, and Leu 174 were responsible for the hydrophobic interactions. Phe 55 was responsible for pi-pi stacking with 50% of the simulation time in the selected trajectory (0-100ns) (Figure 5D2, Supplementary Figure S113B4 and S13C4).

His 236 (interaction fraction of 0.35; hydrophobic interactions), Met 247 (interaction fraction of 0.65; H-bond), and Tyr 248 (interaction fraction of 0.35; hydrophobic interactions) were the amino acids which forms stability in the MMP9-zeilynone complex, which is visualised through the Protein-Ligand Contacts. His 190, His 226, His 230, and His 236 were the polar interaction forming amino acids. Tyr 248 was responsible for the Pi-Pi stacking also (Figure 5E2, Supplementary Figure S13B5 and S13C5).

Trp 194, Gln 205, Phe 369, and Trp 372 were the utmost amino acids which are responsible for the stability of the NOS2-Isozeylanone complex. Trp 194, Phe 369, and Trp 372 were able to form the stable hydrophobic interactions with the interaction fraction of \sim 1.0. Gln 205 was the amino acid for the H-bond and water bridge formation with interaction fraction of 0.5 and 1.0. The ligand-protein contacts were reported with more than 25.0% of the simulation time in the selected trajectory (Figure 5F2, Supplementary Figure S13B6 and S13C6).

3.6. Induced fit docking (IFD)

IFD can be defined as a computational method for the purpose of investigating the conformational and structural changes induced by the receptor-ligand binding, where the receptor is made flexible around the ligand-binding site and the ligand remains rigid.

After performing the IFD of PIK3CA with isozeylanone, the Glidescore had been improved to -10.866 kcal/mol from -10.467 kcal/mol (Glidescore generated by normal XP-mode Glide docking). The IFDScore was found to be -1930.059 . The number of H-bonds had been increased from three (in the normal XP-mode Glide docking) to four (in IFD-generated pose). These residues were Asp 810, Tyr 836, and Val 851. Also, the number of polar interacting residues got increased from four to five, among which the common polar interaction-forming residues were Ser 854, Hie 855, and Thr 856; and the newly formed polar interaction-forming residues were Ser 774 and Gln 859 in the IFD-generated docked pose. Both of the poses were fitted well into the hydrophobic binding pocket formed by the common amino acid residues, viz, Met 772, Trp 780, Ile 800, Tyr 836, Ile 848, Val 850, Val 851, Met 922, and Ile 932. Overall, both docked structures overlapped moderately into the ligand-binding site of PIK3CA (Supplementary Figure Fig. S14A).

The IFD of EGFR with isozeylanone resulted in the improvement of Glidescore from -11.511 kcal/mol (Glidescore

generated by normal XP-mode Glide docking) to -11.533 kcal/mol, and the IFDScore was found to be -660.741 . The number of H-bond forming residues was remained same (three) as it was in the normal XP-mode Glide docking, and these residues were Met 793 and Thr 854. Additionally, there were one pi-cation interaction with the residue Lys 745 that was previously not there in the normal XP-mode docked pose. Also, both of the poses shared common polar interacting residues, viz, Thr 790, Gln 791, and Thr 854. Likewise, both of the poses were fitted well into the hydrophobic binding pocket formed by the common amino acid residues, viz, Leu 718, Val 726, Ala 743, Ile 744, Leu 777, Leu 788, Ile 789, Leu 792, Met 793, Pro 794, Leu 844, Phe 997, and Leu 1001. Additionally, the IFD-generated pose gained one more hydrophobic contact with the residue Cys 775 that was previously not present in the normal XP-mode docked pose. Overall, both docked structures overlapped well into the ligand-binding site of EGFR (Supplementary Figure Fig. S14B).

The IFD of PRKCA with zeilynone resulted in the improvement of Glidescore from -7.905 kcal/mol (Glidescore generated by normal XP-mode Glide docking) to -8.935 kcal/mol, and the IFDScore was found to be -763.171 . However, the number of H-bonds had been decreased from three (in the normal XP-mode Glide docking) to two (in IFD-generated pose), and the residue was Glu 128. The number of polar interaction-forming residues was remained same (three) as it was in the XP-mode Glide docking, and these common residues were Thr 52, Asn 172, and Thr 184. Both of the poses were fitted well into the hydrophobic binding pocket formed by the common amino acid residues, viz, Leu 50, Val 58, Ala 71, Ile 74, Leu 75, Val 105, Met 121, Tyr 123, Val 124, Leu 174, and Phe 328. Additionally, the newly formed hydrophobic interacting residue was Tyr 331. Overall, both docked structures overlapped pretty well into the sitemap-predicted ligand-binding site of PRKCA (Supplementary Figure Fig. S14C).

The IFD of VEGFA with methylnaphthazarin resulted in the improvement of Glidescore from -5.193 kcal/mol (Glidescore generated by normal XP-mode Glide docking) to -6.006 kcal/mol, and the IFDScore was found to be -201.462 . The number of H-bond forming residues was remained same (three) as it was in the normal XP-mode Glide docking, and these residues were Arg 82 and Gln 87. However, it was found that there were two additional types of interactions, i.e., pi-pi stacking and pi-cation interactions, that was not present in the normal XP-mode docked pose. The bioactive, Methylnaphthazarin formed pi-pi stacking interaction with His 90, and formed pi-cation interaction with Lys 84. The polar-interaction and hydrophobic binding pocket-containing residues were also found to be the same as they were in case of normal XP-mode docked pose. Overall, both docked structures overlapped very well into the sitemap-predicted ligand-binding site of VEGFA (Supplementary Figure Fig. S14D).

After performing the IFD of MMP-9 with zeilynone, the Glidescore was improved to -10.367 kcal/mol from -8.670 kcal/mol (Glidescore generated by normal XP-mode Glide docking). The IFDScore was found to be -338.720 . The number of H-bonds had been increased from three (in case

of normal XP-mode Glide docking) to four (in case of IFD). The H-bond interacting residues were Ala 189, Ala 191, and Gln 227. The common polar interactions found between the normal XP-Glide docked pose and IFD-docked pose of Zeylanone with MMP-9 were His 226 and Hie 236. Likewise, both poses were fitted well into the hydrophobic binding pocket formed by the common amino acid residues, viz, Leu 188, Leu 222, Val 223, Ala 242, Leu 243, Tyr 245, Pro 246, Met 247, and Tyr 248. Overall, both docked structures overlapped moderately into the ligand-binding site of MMP-9 (Supplementary Figure Fig. S14E).

After performing the IFD of NOS2 with isozeylanone, the Glidescore had been improved to -8.926 kcal/mol from -8.336 kcal/mol (Glidescore generated by normal XP-mode Glide docking). The IFDScore was found to be -894.647 . The number of H-bonds and pi-pi interactions had been increased from two (in case of normal XP-mode Glide docking) to four (in case of IFD), and from one (in case of normal XP-mode Glide docking) to three (in case of IFD). The new H-bond forming residues in the IFD-generated docked pose were found to be Cys 200 and Tyr 491. Similarly, the new pi-pi stacking interaction forming residues in the IFD-generated docked pose were found to be Phe 369 and Trp 463. However, the number of polar interactions had been decreased from three (in case of normal XP-mode Glide docking) to two (in case of IFD-generated pose). However, the common polar interactions found between the normal XP-Glide docked pose and IFD-docked pose of Isozeylanone with NOS2 were Ser 242 and Asn 370. Both of the poses were fitted well into the hydrophobic binding pocket formed by the common amino acid residues, viz, Trp 194, Ala 197, Cys 200, Leu 209, Val 352, Met 355, Phe 369, Trp 463, Tyr 489, and Tyr 491. Additionally, the IFD-generated docked pose of Isozeylanone formed one more hydrophobic interaction with Ile 244 that was previously not there in the XP-mode Glide docked pose. Overall, both docked structures overlapped moderately into the ligand-binding site of NOS2 (Supplementary Figure Fig. S14F).

All the IFD score of the above discussed ligand receptor complexes were plotted in a bar plot (Supplementary Figure Fig. S14G).

3.7. MM-GBSA calculation

To predict the binding free energies, and to investigate the biophysical basis of molecular recognition of the top three protein-ligand docked complexes against each target, MM-GBSA approach was employed, that provided an account on several individual parameters such as ΔG_{Bind} , ΔG_{Coul} , ΔG_{Hbond} , ΔG_{Lipo} , ΔG_{Solv} , and ΔG_{vdW} (Supplementary Table S14 & Figure S15). MM-GBSA studies have been done in duplicate for the data reliability. It could be seen from the table that for the targets MMP-9 and PRKCA, the net binding free energies followed the same pattern as shown in the XP Glidescores, i.e., the lowest binding energy containing phytoconstituent also showed the lowest net binding free energy, and so on. However, for the rest four targets, the case slightly changed. While for the targets NOS2 and PIK3CA, the

second lowest Glidescore-containing phytoconstituents exhibited the lowest net binding free energies, for the targets VEGFA and EGFR, the third lowest Glidescore-containing phytoconstituents exhibited the lowest net binding free energies. It could be seen from the ΔG_{vdW} value (data in supporting information) that it contributed significantly towards the net binding free energy (ΔG_{Bind} , data in supporting information) of the complexes.

3.8. In silico physicochemical and ADME/T studies

The bioactive phytoconstituents having lowest binding energy with all six target proteins were found to be isozeylanone, 2-(1-hydroxy-1-methyl-ethyl)-9-methoxy-1,8-dioxo-dicyclopenta-b-g-Naphthalene-4,10-dione, and zeylanone, whose in silico ADME/T properties were predicted using the QikProp program of Schrödinger 2017-2 and the SwissADME online server, and are tabulated in the Supplementary Table S14. All of the QikProp-predicted properties were found to be in the acceptable range. The molecular weights, percent human oral absorptions, surface area, and volumes of each bioactives were found to be in the acceptable range. These phytoconstituents possessed the Log P, polarizability, and surface area within the acceptable range, too.

From the SwissADME-predicted properties, it could be shown from the egg-boiled diagram that all three bioactives (Supplementary Figure S16) were not found to be CNS-active. However, any of them were not predicted as P-glycoprotein (PGP)-substrate. Eventually, all of them exhibited no violation of Lipinski's, Ghose's, Veber's, Egan's, and Muegge's (Bayer) rules. Moreover, the top two phytoconstituents, i.e., Isozeylanone and 2-(1-hydroxy-1-methyl-ethyl)-9-methoxy-1,8-dioxo-dicyclopenta-b-g-Naphthalene-4,10-dione were found to be the inhibitor of three of Cytochrome P450 (CYP1A2, CYP2C6, and CYP3A4) enzymes. Whereas Zeylanone was found as a non-inhibitor of all subtype of CYP enzymes. All-in-all, these phytoconstituents can be processed for further studies due to their drug-likeness and considerable pharmacokinetic property.

From ProTox-II-predicted data, it was found that both isozeylanone and 2-(1-hydroxy-1-methyl-ethyl)-9-methoxy-1,8-dioxo-dicyclopenta-b-g-Naphthalene-4,10-dione fell in the 'Toxicity class IV (harmful if swallowed [$300 < \text{LD50} \leq 2000$])', while zeylanone fell in the 'Toxicity class II (fatal if swallowed [$5 < \text{LD50} \leq 50$])'. The predicted LD50 for the three phytoconstituents were found to be 1000, 450, and 34 mg/kg, respectively (Supplementary Figure Fig. S17).

4. Conclusion

Results of the network pharmacology analysis revealed that the potential mechanisms of treatment of hemorrhoids are related to the processes including cell migration, regulation of cell population proliferation, cell motility, and apoptosis and those biological actions are synchronized by the cancer, relaxin signalling pathways, focal adhesion, Rap1 signalling pathway and calcium signalling pathway. The molecular docking outcomes reveal that the active ingredients of P.

zeylanica binds with the key target proteins, such as, PIK3CA, EGFR, PRKCA, VEGFA, MMP-9 and NOS2 in the ambience of hemorrhoids. The study has some shortcoming owing to the experimental validation deficit, but it can encourage the *in-vitro* or *in-vivo* studies. Altogether, this study unveil the systemic biological profiles of *P. zeylanica*. However, future experimental studies are required to validate the current findings.

Acknowledgements

The authors are thankful to the Science and Engineering Board (SERB), Department of Science and Technology, India for providing support for the completion of the research work with Grant No. SRG/2021/001631 under Start-up Research Grant (SRG). The authors are also thankful to the Principal, Dr. B. C. Roy College of Pharmacy and Allied Health Sciences, Durgapur for the encouragement of this work.

Disclosure statement

No potential conflict of interest was reported by the author(s).

Funding

Yadu Nandan Dey wishes to thank Science and Engineering Research Board, Department of Science and Technology for providing financial support to carry out the project through Grant Number SRG/2021/001631.

Author contributions

Y.N.D. contributed to the generation of concept, and supervision of the research work and drafting the research paper. A.N. contributed significantly in the network analysis and drafting the research paper. A.N. and A.D. contributed in the molecular docking and dynamics analysis. T.N. assisted in network analysis and drafting of manuscript. All authors of this manuscript have read and approved the manuscript for submission.

Data availability statement

The datasets supposing the current study are available in public databases from IMPPAT, PUBMED, PubChem, Swiss Target Prediction, BindingDB, DisGeNET, GeneCards, OMIM, UniProt, STRING, ShinyGO, RCSB PDB, and SwissADME. All the analysed data during the current study are available in the manuscript and [supplementary material](#).

References

- Abdizadeh, R., Heidarian, E., Hadizadeh, F., & Abdizadeh, T. (2020). Investigation of pyrimidine analogues as xanthine oxidase inhibitors to treat of hyperuricemia and gout through combined QSAR techniques, molecular docking and molecular dynamics simulations. *Journal of the Taiwan Institute of Chemical Engineers*, 113, 72–100. <https://doi.org/10.1016/j.jtice.2020.08.028>
- Auti, P. S., Nandi, A., Kumari, V., & Paul, A. T. (2022). Design, synthesis, biological evaluation and molecular modelling studies of oxoacetamide warhead containing indole-quinazolinone based novel hybrid analogues as potential pancreatic lipase inhibitors. *New Journal of Chemistry*, 46(24), 11648–11661. <https://doi.org/10.1039/D2NJ01210C>
- Bowers, K. J., Chow, E., Xu, H., Dror, R. O., Eastwood, M. P., Gregersen, B. A., ... Shaw, D. E. (2006). Scalable algorithms for molecular dynamics simulations on commodity clusters. In *SC '06: Proceedings of the 2006 ACM/IEEE Conference on Supercomputing*: Vol. November (pp. 84–95). Retrieved from [papers://c33b182f-cf88-47e8-a9c5-ad67b5626483/Paper/p1310](https://doi.org/10.1145/1140000.1140000)
- Camodeca, C., Nuti, E., Tepshi, L., Boero, S., Tuccinardi, T., Stura, E. A., Poggi, A., Zocchi, M. R., & Rossello, A. (2016). Discovery of a new selective inhibitor of A Disintegrin and Metalloprotease 10 (ADAM-10) able to reduce the shedding of NKG2D ligands in Hodgkin's lymphoma cell models. *European Journal of Medicinal Chemistry*, 111, 193–201. <https://doi.org/10.1016/j.ejmech.2016.01.053>
- Chattaraj, B., Khanal, P., Nandi, A., Das, A., Sharma, A., Mitra, S., & Dey, Y. N. (2023). Network pharmacology and molecular modelling study of Enhydra fluctuans for the prediction of the molecular mechanisms involved in the amelioration of nephrolithiasis. *Journal of Biomolecular Structure & Dynamics*, 1–11. <https://doi.org/10.1080/07391102.2023.2189476>
- Chattaraj, B., Nandi, A., Das, A., Baidya, A., Mahata, S., Chowdhury, A., Mitra, S., Roy, S., Chakraborty, S., & Dey, Y. N. (2023). Enhydra fluctuans Lour. aqueous extract inhibited the growth of calcium phosphate crystals: An in vitro study. *Food Chemistry Advances*, 2(August 2022), 100287. <https://doi.org/10.1016/j.focha.2023.100287>
- Chattaraj, B., Nandi, A., Das, A., Sharma, A., Dey, Y. N., Kumar, D., & Mogana, R. (2022). Inhibitory activity of *Enhydra fluctuans* Lour. on calcium oxalate crystallisation through in silico and in vitro studies. *Frontiers in Pharmacology*, 13(January), 982419. <https://doi.org/10.3389/fphar.2022.982419>
- Checker, R., Sharma, D., Sandur, S. K., Khanam, S., & Poduval, T. B. (2009). Anti-inflammatory effects of plumbagin are mediated by inhibition of NF-kappaB activation in lymphocytes. *International Immunopharmacology*, 9(7-8), 949–958. <https://doi.org/10.1016/j.intimp.2009.03.022>
- Cheng, Y., Li, H., Wu, D., Hu, Y., Li, J., Yang, Y., Li, J., Zhou, H., Zhang, H., Xie, C., & Yang, C. (2023). Anti-inflammatory polyoxygenated cyclohexene derivatives from *Uvaria macclurei*. *Phytochemistry*, 214(July), 113797. <https://doi.org/10.1016/j.phytochem.2023.113797>
- Chowdhury, A., Patel, S., Sharma, A., Das, A., Meshram, P., & Shard, A. (2020). A perspective on environmentally benign protocols of thiazole synthesis. *Chemistry of Heterocyclic Compounds*, 56(4), 455–463. <https://doi.org/10.1007/s10593-020-02680-x>
- Chung, Y. C., Hou, Y. C., & Pan, A. C. H. (2004). Endoglin (CD105) expression in the development of haemorrhoids. *European Journal of Clinical Investigation*, 34(2), 107–112. <https://doi.org/10.1111/j.1365-2362.2004.01305.x>
- Daina, A., Michielin, O., & Zoete, V. (2017). (2017). SwissADME: A free web tool to evaluate pharmacokinetics, drug-likeness and medicinal chemistry friendliness of small molecules. *Scientific Reports*, 7(1), 42717. <https://doi.org/10.1038/srep42717>
- Dwivedi, S. (1997). Effect of *Plumbago zeylanica* in hyperlipidemic rabbits and its modification by vitamin E. *Indian Journal of Pharmacology*, 29(2), 138.
- Edition, F. (2016). *the ayurvedic pharmacopoeia of India*.
- Garcin, E. D., Arvai, A. S., Rosenfeld, R. J., Kroeger, M. D., Crane, B. R., Andersson, G., Andrews, G., Hamley, P. J., Mallinder, P. R., Nicholls, D. J., St-Gallay, S. A., Tinker, A. C., Gensmantel, N. P., Mete, A., Cheshire, D. R., Connolly, S., Stuehr, D. J., Aberg, A., Wallace, A. V., Tainer, J. A., & Getzoff, E. D. (2008). Anchored plasticity opens doors for selective inhibitor design in nitric oxide synthase. *Nature Chemical Biology*, 4(11), 700–707. <https://doi.org/10.1038/nchembio.115>
- Genheden, S., & Ryde, U. (2015). The MM/PBSA and MM/GBSA methods to estimate ligand-binding affinities. *Expert Opinion on Drug Discovery*, 10(5), 449–461. <https://doi.org/10.1517/17460441.2015.1032936>
- Gulati, K., Guhathakurta, S., Joshi, J., Rai, N., & Ray, A. B. (2016). Cytokines and their role in health and disease: A brief overview. *MOJ Immunology*, 4(2), 1–9. <https://doi.org/10.15406/moji.2016.04.00121>
- Hafeez, B. B., Zhong, W., Fischer, J. W., Mustafa, A., Shi, X., Meske, L., Hong, H., Cai, W., Havighurst, T., Kim, K., & Verma, A. K. (2013). Plumbagin, a medicinal plant (*Plumbago zeylanica*)-derived 1,4-naphthoquinone, inhibits growth and metastasis of human prostate cancer PC-3M-luciferase cells in an orthotopic xenograft mouse model. *Molecular Oncology*, 7(3), 428–439. <https://doi.org/10.1016/j.molonc.2012.12.001>
- Han, W., Wang, Z. j., Zhao, B., Yang, X. q., Wang, D., Wang, J. p., ... Hung, Y. t (2005). Pathologic change of elastic fibers with difference of microvessel density and expression of angiogenesis-related

- proteins in internal hemorrhoid tissues. *Zhonghua Wei Chang Wai Ke Za Zhi = Chinese Journal of Gastrointestinal Surgery*, 8(1), 56–59. <https://europepmc.org/article/med/16149003>
- Hong, Z., Zhang, T., Zhang, Y., Xie, Z., Lu, Y., Yao, Y., Yang, Y., Wu, H., & Liu, B. (2021). Reveals of candidate active ingredients in *Justicia* and its anti-thrombotic action of mechanism based on network pharmacology approach and experimental validation. *Scientific Reports*, 11(1), 17187. <https://doi.org/10.1038/s41598-021-96683-z>
- Jacobson, M. P., Pincus, D. L., Rapp, C. S., Day, T. J. F., Honig, B., Shaw, D. E., & Friesner, R. A. (2004). A hierarchical approach to all-atom protein loop prediction. *Proteins*, 55(2), 351–367. <https://doi.org/10.1002/prot.10613>
- Kobialka, P., Sabata, H., Vilalta, O., Gouveia, L., Angulo-Urarte, A., Muixí, L., Zanoncello, J., Muñoz-Aznar, O., Olacriegui, N. G., Fanlo, L., Esteve-Codina, A., Lavarino, C., Javierre, B. M., Celis, V., Rovira, C., López-Fernández, S., Baselga, E., Mora, J., Castillo, S. D., & Graupera, M. (2022). The onset of PI3K-related vascular malformations occurs during angiogenesis and is prevented by the AKT inhibitor miransertib. *EMBO Molecular Medicine*, 14(7), e15619. <https://doi.org/10.15252/emmm.202115619>
- Lin, L. C., Yang, L. L., & Chou, C. J. (2003). Cytotoxic naphthoquinones and plumbagic acid glucosides from *Plumbago zeylanica*. *Phytochemistry*, 62(4), 619–622. [https://doi.org/10.1016/S0031-9422\(02\)00519-8](https://doi.org/10.1016/S0031-9422(02)00519-8)
- Liu, T., Zhou, H., Lu, H., Luo, C., Wang, Q., Peng, Y., Yang, W., & Xin, Y. (2021). MiR-4729 regulates TIE1 mRNA m6A modification and angiogenesis in hemorrhoids by targeting METTL14. *Annals of Translational Medicine*, 9(3), 232–232. <https://doi.org/10.21037/atm-20-3399>
- Lohsiriwat, V. (2012). Hemorrhoids: From basic pathophysiology to clinical management. *World Journal of Gastroenterology*, 18(17), 2009–2017. <https://doi.org/10.3748/wjg.v18.i17.2009>
- Madan, A., Garg, M., Satija, G., Sharma, B., Shaquiquzzaman, M., Akhter, M., Iqbal, A., Khan, M. A., Parvez, S., Das, A., Sheikh, K. A., & Alam, M. M. (2023). SAR based review on diverse heterocyclic compounds with various potential molecular targets in the fight against Covid-19: A medicinal chemist perspective. *Current Topics in Medicinal Chemistry*, 23(14), 1319–1339. <https://doi.org/10.2174/1568026623666230126104156>
- Makhal, P. N., Nandi, A., & Kaki, V. R. (2021). Insights into the recent synthetic advances of organoselenium compounds. *ChemistrySelect*, 6(4), 663–679. <https://doi.org/10.1002/slct.202004029>
- Margetis, N. (2019). Pathophysiology of internal hemorrhoids. *Annals of Gastroenterology*, 32(3), 264–272. <https://doi.org/10.20524/aog.2019.0355>
- Meng, F., Chen, X., Liu, H., Zhang, L., Yu, T., & Xie, M. (2022). Fulvestrant, an estrogen receptor inhibitor, relieves postoperative hemorrhoid edema via up-regulation of miR-424-5p. *Tropical Journal of Pharmaceutical Research*, 21(5), 1101–1107. <https://doi.org/10.4314/tjpr.v21i5.27>
- Methot, J. L., Achab, A., Christopher, M., Zhou, H., McGowan, M. A., Trotter, B. W., Fradera, X., Lesburg, C. A., Goldenblatt, P., Hill, A., Chen, D., Otte, K. M., Augustin, M., Shah, S., & Katz, J. D. (2020). Optimization of versatile oxindoles as selective PI3K δ inhibitors. *ACS Medicinal Chemistry Letters*, 11(12), 2461–2469. <https://doi.org/10.1021/acsmmedchemlett.0c00441>
- Nandi, A., Das, A., Dey, Y. N., & Roy, K. K. (2023). The abundant phytocannabinoids in rheumatoid arthritis: Therapeutic targets and molecular processes identified using integrated bioinformatics and network pharmacology. *Life*, 13(3), 700. <https://doi.org/10.3390/life13030700>
- Nandi, A., Das, A., Lin, W., & Chakraborty, P. (n.d.). Chapter 6: Antiviral drugs – In past and in current pandemics.
- Parveen, D., Das, A., Amin, S., Alam, M. M., Akhter, M., Ahmed Khan, M., Ali, R., Anwer, T., Sheikh, K. A., Azam, F., & Shaquiquzzaman, M. (2023). Effectiveness of estrogen and its derivatives over dexamethasone in the treatment of COVID-19. *Journal of Biomolecular Structure & Dynamics*, 0(0), 1–17. <https://doi.org/10.1080/07391102.2023.2205944>
- Patel, S., Das, A., Meshram, P., Sharma, A., Chowdhury, A., Jariyal, H., Datta, A., Sarmah, D., Nalla, L. V., Sahu, B., Khairnar, A., Bhattacharya, P., Srivastava, A., & Shard, A. (2021). Pyruvate kinase M2 in chronic inflammations: A potpourri of crucial protein–protein interactions. *Cell Biology and Toxicology*, 37(5), 653–678. <https://doi.org/10.1007/s10565-021-09605-0>
- Porwal, A., Kundu, G. C., Bhagwat, G., & Butti, R. (2021). Polyherbal formulation Anoaac-H suppresses the expression of RANTES and VEGF for the management of bleeding hemorrhoids and fistula. *Molecular Medicine Reports*, 24(4), 1–8. <https://doi.org/10.3892/mmr.2021.12376>
- QikProp | Schrödinger. (n.d.). Retrieved August 19, 2022, from <https://www.schrodinger.com/products/qikprop>
- Sandeep, G., Dheeraj, A., Sharma, N. K., Jhade, D., & Bharti, A. (2011). Effect of plumbagin free alcohol extract of *Plumbago zeylanica* Linn. root on reproductive system of female Wistar rats. *Asian Pacific Journal of Tropical Medicine*, 4(12), 978–984. [https://doi.org/10.1016/S1995-7645\(11\)60230-7](https://doi.org/10.1016/S1995-7645(11)60230-7)
- Satyavati, G. V., Gupta, A. K., Tandon, N., & Seth, S. D. (1987). *Medicinal plants of India* (1st ed., Vol. 2). Indian Council of Medical Research.
- Sharma, P. C., Yelne, M. B., Dennis, T. J., Joshi, A., & Billore, K. V. (2000). *Database on medicinal plants used in Ayurveda*. <https://doi.org/10.3/JQUERY-UJJS>
- Sheikh, P., Régnier, C., Goron, F., & Salmat, G. (2020). The prevalence, characteristics and treatment of hemorrhoidal disease: Results of an international web-based survey. *Journal of Comparative Effectiveness Research*, 9(17), 1219–1232. <https://doi.org/10.2217/cer-2020-0159>
- Shrimali, M., Jain, D. C., Darokar, M. P., & Sharma, R. P. (2001). Central nervous system stimulatory action from the root extract of *Plumbago zeylanica* in rats. *Phytotherapy Research*, 15(2), 153–156. <https://doi.org/10.1002/ptr.702>
- Shrivastava, L., Silva Borges, G. d., & Shrivastava, R. (2018). Clinical efficacy of a dual action, topical anti-edematous and anti-inflammatory device for the treatment of external hemorrhoids. *Clinical and Experimental Pharmacology*, 08(01), 1–7. <https://doi.org/10.4172/2161-1459.1000246>
- Sidhu, G. S., & Sankaram, A. V. B. (1971). A new biplumbagin and 3-chloroplumbagin from *Plumbago zeylanica*. *Tetrahedron Letters*, 12(26), 2385–2388. [https://doi.org/10.1016/S0040-4039\(01\)96870-4](https://doi.org/10.1016/S0040-4039(01)96870-4)
- Sogabe, S., Kawakita, Y., Igaki, S., Iwata, H., Miki, H., Cary, D. R., Takagi, T., Takagi, S., Ohta, Y., & Ishikawa, T. (2013). Structure-based approach for the discovery of pyrrolo[3,2-d] pyrimidine-based EGFR T790M/L858R mutant inhibitors. *ACS Medicinal Chemistry Letters*, 4(2), 201–205. <https://doi.org/10.1021/ml300327z>
- Song, S., Zhou, J., Li, Y., Liu, J., Li, J., & Shu, P. (2022). Network pharmacology and experimental verification based research into the effect and mechanism of Aucklandia Radix–Amomi Fructus against gastric cancer. *Scientific Reports*, 12(1), 9401. <https://doi.org/10.1038/s41598-022-13223-z>
- Sun, Z., Yang, S., Xu, C., Yi, F., Cao, L., Tian, Y., Lin, J., & Xu, X. (2021). Concise total synthesis of (+)-Zeylenone with antitumor activity and the structure–activity relationship of its derivatives. *Bioorganic Chemistry*, 116(September), 105333. <https://doi.org/10.1016/j.bioorg.2021.105333>
- Tutone, M., Pibiri, I., Lentini, L., Pace, A., & Almerico, A. M. (2019). Deciphering the nonsense readthrough mechanism of action of ataluren: An in silico compared study. *ACS Medicinal Chemistry Letters*, 10(4), 522–527. https://doi.org/10.1021/ACSMEDCHEMLETT.8B00558/SUPPL_FILE/ML8B00558_SI_001.PDF
- Van Cruysen, H., Giaccone, G., & Hoekman, K. (2005). Epidermal growth factor receptor and angiogenesis: Opportunities for combined anti-cancer strategies. *International Journal of Cancer*, 117(6), 883–888. <https://doi.org/10.1002/ijc.21479>
- Wang, J., Li, B., Zhang, X., Hu, Q., Yu, W., Wang, H., Duan, D., Li, J., & Zhao, B. (2019). Docking and molecular dynamics studies on the mechanism of phospholipase D-mediated transphosphatidylation to construct the reaction kinetic model: Application in phosphatidylserine production. *Journal of the Taiwan Institute of Chemical Engineers*, 96, 82–92. <https://doi.org/10.1016/j.jtice.2018.12.012>
- Wojdasiewicz, P., Poniatowski, Ł. A., & Szukiewicz, D. (2014). The role of inflammatory and anti-inflammatory cytokines in the pathogenesis of osteoarthritis. *Mediators of Inflammation*, 2014, 561459–561419. <https://doi.org/10.1155/2014/561459>
- Xu, H., Czerwinski, P., Hortmann, M., Sohn, H. Y., Förstermann, U., & Li, H. (2008). Protein kinase C α promotes angiogenic activity of human

- endothelial cells via induction of vascular endothelial growth factor. *Cardiovascular Research*, 78(2), 349–355. <https://doi.org/10.1093/cvr/cvm085>
- Xu, X., Shi, J., Gao, H., & Li, Q. (2018). Zeylenone inhibits proliferation and promotes apoptosis in ovarian carcinoma cells via Janus kinase 2/signal transducers and activators of transcription 3 pathways. *The Journal of Obstetrics and Gynaecology Research*, 44(8), 1451–1457. <https://doi.org/10.1111/jog.13690>
- Yang, S., Liao, Y., Li, L., Xu, X., & Cao, L. (2018). Zeylenone induces mitochondrial apoptosis and inhibits migration and invasion in gastric cancer. *Molecules (Basel, Switzerland)*, 23(9), 2149. <https://doi.org/10.3390/molecules23092149>
- Yang, S., Xiao, H., Sun, Y., & Cao, L. (2021). Zeylenone synergizes with cisplatin in osteosarcoma by enhancing DNA damage, apoptosis, and necrosis via the Hsp90/AKT/GSK3 β and Fanconi anaemia pathway. *Phytotherapy Research: PTR*, 35(10), 5899–5918. <https://doi.org/10.1002/ptr.7299>
- Zeng, S., Zhu, B., Zeng, J., Wu, W., & Jiang, C. (2018). Zeylenone represses the progress of human prostate cancer by downregulating the Wnt/ β -catenin pathway. *Molecular Medicine Reports*, 18(6), 5572–5578. <https://doi.org/10.3892/mmr.2018.9564>
- Zhang, L., Huo, X., Liao, Y., Yang, F., Gao, L., & Cao, L. (2017). Zeylenone, a naturally occurring cyclohexene oxide, inhibits proliferation and induces apoptosis in cervical carcinoma cells via PI3K/AKT/mTOR and MAPK/ERK pathways. *Scientific Reports*, 7(1), 1669. <https://doi.org/10.1038/s41598-017-01804-2>
- Zhang, M., Yang, J., Zhao, X., Zhao, Y., & Zhu, S. (2021). Network pharmacology and molecular docking study on the active ingredients of qidengmingmu capsule for the treatment of diabetic retinopathy. *Scientific Reports*, 11(1), 7382. <https://doi.org/10.1038/s41598-021-86914-8>